

2019-07-01

Jurassic shift from abiotic to biotic control on marine ecological success

Eichenseer, K

<http://hdl.handle.net/10026.1/14472>

10.1038/s41561-019-0392-9

Nature Geoscience

Nature Research

All content in PEARL is protected by copyright law. Author manuscripts are made available in accordance with publisher policies. Please cite only the published version using the details provided on the item record or document. In the absence of an open licence (e.g. Creative Commons), permissions for further reuse of content should be sought from the publisher or author.

This is the author's accepted manuscript. The final published version of this work is published by in *Nature Geoscience* available at: DOI 10.1038/s41561-019-0392-9. This work is made available online in accordance with the publisher's policies. Please refer to any applicable terms of use of the publisher.

accepted on the 22nd of May 2019

Jurassic shift from abiotic to biotic control on marine ecological success

Kilian Eichenseer¹, Uwe Balthasar¹, Christopher W. Smart¹, Julian Stander², Kristian A. Haaga^{3,4,5}, Wolfgang Kiessling⁶

¹ School of Geography, Earth and Environmental Sciences, University of Plymouth, Drake Circus, Plymouth PL4 8AA, UK

² School of Computing, Electronics and Mathematics, University of Plymouth, Drake Circus, Plymouth PL4 8AA, UK

³ Department of Earth Science, University of Bergen, N-5020 Bergen, Norway

⁴ Bjerknes Centre for Climate Research, PO Box 7803, NO-5020 Bergen, Norway

⁵ K.G. Jebsen Centre for Deep Sea Research, P.O. Box 7803, N-5020, Bergen, Norway

⁶ GeoZentrum Nordbayern, Department of Geography and Geosciences, Universität Erlangen-Nürnberg, Loewenichstraße 28, 91054 Erlangen, Germany

Environmental change and biotic interactions both govern the evolution of the biosphere, but the relative importance of these drivers over geological time remains largely unknown. Previous work suggests that, unlike environmental parameters, diversity dynamics differ profoundly between the Palaeozoic and post-Palaeozoic eras. Here we use the fossil record to test the hypothesis that the influence of ocean chemistry and climate on the ecological success of marine calcifiers decreased throughout the Phanerozoic eon. Marine calcifiers build skeletons of calcite or aragonite, and the precipitation of these calcium carbonate polymorphs is governed by the magnesium-to-calcium ratio and temperature in abiotic systems. We developed an environmental forcing model based on secular changes of ocean chemistry and temperature and assessed how well the model predicts the proliferation of skeletal taxa with respect to calcium carbonate polymorphs. Abiotic forcing governs the ecological success of aragonitic calcifiers from the Ordovician to the Middle Jurassic, but not thereafter. This regime shift coincides with the proliferation of calcareous plankton in the mid-Mesozoic. The deposition of biomineralizing plankton on the ocean floor buffers CO₂ excursions and stabilizes Earth's biochemical cycle, and thus mitigates the evolutionary impact of environmental change on the marine biota.

Dramatic shifts in the success of dominant animal groups in Earth history abound in the fossil record¹ and there are numerous Phanerozoic-scale macroevolutionary trends. Traits such as body size, the metabolic rate of dominant taxonomic groups, and physiological buffering capacity have increased over the course of the Phanerozoic²⁻⁵. As a consequence, biotic interactions may have increased as well⁶⁻⁹. In contrast, climate and seawater composition show a cyclical behaviour rather than Phanerozoic-scale trends^{10,11}. The biosphere has evolved to cushion some environmental variability: for example, the buffering of ocean

chemistry has increased due to the mid-Mesozoic ascent of calcifying plankton¹². Perturbations of the carbon cycle have fallen in amplitude, particularly since the mid-Mesozoic¹³ (Fig. 1d), and extinction rates have decreased towards the present¹⁴ (Fig. 1e). Accordingly, we hypothesize that the evolutionary importance of the abiotic environment, relative to intrinsic, biotic factors, has declined through geological time.

We tested this hypothesis using the vast fossil record of marine calcifiers. In the inorganic formation of calcium carbonate (CaCO_3), high Mg/Ca ratios and high temperatures have been shown to favour the precipitation of aragonite over calcite, and *vice versa*¹⁵. Across the Phanerozoic, tectonically driven changes in sea water chemistry and climate have caused aragonite and calcite favouring conditions to alternate, giving rise to episodes of “aragonite seas” and “calcite seas”^{10,16} (Fig. 1b). The skeletal mineralogy of calcifying organisms is strongly tied to phylogenetic history, but the *de novo* acquisition of biominerals, skeletal composition, skeletal production, and growth rates of many marine calcifiers are affected by the Mg/Ca ratio and temperature of the surrounding sea water¹⁷⁻²¹, analogous to inorganic CaCO_3 formation. If aragonite and calcite seas were influential in the evolution of marine calcifiers, we expect a correspondence of aragonite sea conditions with greater success of aragonitic taxa.

Aragonite - calcite seas and the success of marine calcifiers

We combine a model of past Mg/Ca ratios²² (Fig. 1b) with $\delta^{18}\text{O}$ temperature reconstructions²³ (Fig. 1c) to quantify *aragonite sea intensity* (*ASI*) in 85 post-Cambrian stages. The *ASI* is parametrized from experimental data¹⁵ via multiple regression. We contrast *ASI* with a measure of the environmental occupancy, or success, of aragonitic genera relative to all calcifying genera (*SCOR_{ara}*), calculated with the Summed Common species Occurrence Rate

(*SCOR*)²⁴. Given that novel acquisitions of calcium carbonate skeletons are rare and that switches in skeletal mineralogy are largely restricted to a few clades^{20,21,25}, changes in *SCOR_{ara}* reflect predominantly the differential success of aragonitic taxa, rather than changing mineralogies within calcifying clades (Supplementary Materials S6). Although the lower preservation potential of aragonitic taxa may lead to underestimate the abundance of aragonitic taxa²⁶, we find that the completeness of the record of aragonitic and calcitic genera is not significantly different (Wilcoxon signed-rank test: $p = 0.28$, Supplementary Materials S3). The strength of abiotic controls on marine calcifiers is assessed by estimating linear models of *SCOR_{ara}* against *ASI* using generalised least squares (GLS) to account for temporal autocorrelation, and by convergent cross mapping (CCM) to detect causal coupling²⁷ (*Methods*).

Visual inspection of the *SCOR_{ara}* and *ASI* time series suggests an association in the Ordovician – Carboniferous and again in the early Mesozoic, but not for most of the Mesozoic and Cenozoic (Fig. 1a). A linear model of *SCOR_{ara}* against *ASI* is significant in the Palaeozoic ($R^2 = 0.15$, $p = 0.017$, Table 1), and not in the Mesozoic – Cenozoic ($R^2 < 0.01$, $p = 0.68$), suggesting a decreasing dependence of ecological success on relevant environmental conditions in the Mesozoic. In the entire Ordovician – Pleistocene data, the linear relationship is not significant ($R^2 < 0.01$, $p = 0.70$), however the sharp rise of *SCOR_{ara}* across the Permian-Triassic makes estimating linear models across this boundary problematic.

We used a Bayesian approach to identify the timing of the changes in the relationship between *SCOR_{ara}* and *ASI* (see *Methods*). This analysis identifies the Permian-Triassic boundary as the strongest change point of the entire Phanerozoic time series (supported by 100 % posterior probability; Fig. 2a, purple bar). When evaluating only the Palaeozoic time

series, the Carboniferous – Permian boundary shows the strongest change (73% probability; Fig. 2a, red bars), whereas no unambiguous single change point is found for the Mesozoic – Cenozoic time series (all probabilities <25%; Fig. 2a, green bars).

To evaluate the possibility of a gradual change, we fitted linear models of $SCOR_{ara}$ against ASI from the Triassic onwards, adding successively more stages towards the present, and repeated the same process with the Palaeozoic data, separately. The relationship of $SCOR_{ara}$ and ASI is consistently strong in the Palaeozoic, with a weakening around the Carboniferous – Permian boundary (Figure 2b). In the Mesozoic, a positive linear relationship persists up to the Middle Jurassic, although with lower statistical support. No relationship is supported from the Late Jurassic onwards. The relationship of $SCOR_{ara}$ and ASI evolves in a similar way when $SCOR_{ara}$ is calculated only in the subset of organisms which are considered especially responsive to physiochemical changes in the environment (Supplementary Fig. S7)^{2,25,28}.

These results are reinforced by using CCM, a technique developed to detect causal coupling between time series by quantifying the extent to which a putative response time series can be used to predict a driver time series²⁷ (see *Methods*). If this prediction is successful beyond some appropriate null hypothesis (*Methods*), we take it as evidence of dynamical coupling. Applying CCM in expanding time windows, we find a significant dynamical influence of ASI on $SCOR_{ara}$ in the Ordovician - Jurassic (Fig. 2c), implying a causal link between aragonite-calcite sea conditions and $SCOR_{ara}$ in this part of the record. Following a maximum in the early Jurassic (Sinemurian), the CCM prediction skill decreases gradually until the Early Cretaceous and remains low thereafter. This decline indicates a weakening influence of ASI on the success of marine calcifiers towards the present.

Our findings corroborate the hypothesis of a decreasing environmental influence on marine calcifiers' success. The correlation of aragonite-calcite seas and the success of aragonitic calcifiers decreased chiefly in two episodes: Around the Carboniferous-Permian boundary, and in a second episode centred in the Middle Jurassic (Fig 2). Permian seawater had an unusually high CaCO_3 saturation^{12,29}. All else being equal, higher CaCO_3 saturation facilitates calcification³⁰ and tends to shift the CaCO_3 polymorph balance in favour of calcite³¹. Consequently, calcifiers with a calcitic skeleton performed better than predicted by *ASI* when the CaCO_3 saturation state rose in the Permian. Calcitic taxa, particularly brachiopods, became more successful across the Carboniferous – Permian boundary (Supplementary Fig. S8, a detailed discussion of the relative success of the major taxonomic groups of marine calcifiers is provided in the Supplementary Materials). The influence of *ASI* on $SCOR_{ara}$ decreased but their correlation remained positive within the Permian (Fig. 2b, Table 1). Although CaCO_3 saturation state probably remained high during the Triassic³², *ASI* continued to affect $SCOR_{ara}$ in the early Mesozoic, but not thereafter.

The role of calcifying plankton

In the mid-Mesozoic, the Earth-Life system was revolutionised by the rise of calcifying plankton¹². Before the widespread occurrence of planktonic calcifiers, CaCO_3 precipitation was largely confined to the continental shelves and linked to the success of benthic calcifiers such as corals and brachiopods. The evolutionary success of calcifying plankton, especially of coccolithophores³³, shifted the carbonate factory from the shelves to the open ocean. Calcareous tests sink to the ocean floor and either dissolve or accumulate, depending on the local CaCO_3 saturation state. Since the proliferation of planktonic calcifiers, changes in the atmospheric and oceanic CO_2 content have been compensated on geologically short time

scales by increased CaCO_3 deposition or dissolution in the deep sea³⁴. The evolutionary impact of episodes of severe climatic change with associated ocean acidification such as the Palaeocene-Eocene Thermal Maximum has been less severe than comparable events in the Palaeozoic and early Mesozoic^{35,36}, possibly a consequence of the increased ocean buffering^{12,37}

Producing a skeleton out of *sync* with aragonite-calcite sea conditions may be costly especially when CaCO_3 secretion is impeded by ocean acidification. Enhanced ocean buffering after the proliferation of calcifying plankton can explain the diminished response of marine calcifiers to changing aragonite-calcite sea conditions after the mid-Jurassic. Several key events in the evolution of calcifying plankton fall into the Middle – Late Jurassic. Planktonic foraminifera first appear in the fossil record during the Lower Jurassic, but the first known deep water carbonate oozes composed of planktonic foraminifera date back to the Middle Jurassic^{38,39}. The thick-walled coccolithophore genus *Watznaueria* diversified in the early Middle Jurassic, resulting in an increase of coccolith flux to the sediment by two orders of magnitude⁴⁰. Nannofossil deposits from the Tethys ocean show that coccolithophores colonised the open ocean during the Late Jurassic and became abundant enough to affect the marine carbonate system⁴¹.

A new evolutionary regime

Beyond skeletal mineralogy, there is evidence for a wider regulatory change of evolutionary patterns and environmental state shifts in the mid-Phanerozoic. Devastating extinctions in the Late Permian – early Mesozoic overturned the taxonomic composition of marine calcifiers^{36,42} and favoured the survival of active and physiologically buffered animals^{28,43}. As a consequence, the dominant, modern marine biota are less vulnerable to abiotic stressors

than their Palaeozoic counterparts⁴³, and individual energy budgets of bivalves and gastropods increased throughout the early Mesozoic^{3,5}. This rise in available metabolic energy may have helped absorb the cost of secreting a shell out of *sync* with aragonite-calcite sea conditions.

The Mesozoic rise of plankton such as foraminifera³⁸, coccolithophores, and dinoflagellates⁴⁴ had an additional effect on the bio-geosphere: tests of phytoplankton act as ballast, increasing its sinking velocity and increasing the depth at which organic carbon is oxidised, which in turn can explain the much lower prevalence of anoxia on Mesozoic and Cenozoic shelves⁴⁵. Increasing oxygenation of shallow ocean water is indicated from the Jurassic onwards by iodine-to-calcium ratios⁴⁶ (Fig. 1f). Well-oxygenated shelves stabilise the carbon cycle by reducing the impact of sea level changes on the burial capacity of organic carbon¹³, thus decreasing the potential for catastrophic environmental change. Increasing oxygen availability also allows for higher metabolic rates and more active modes of life in the shelf biota, as has been inferred for the mid-Mesozoic⁴⁷ and may have increased the pace of escalation in evolution⁴⁸. The onset of a persistent diversity rise in the Middle Jurassic agrees with this interpretation (Fig. 1g).

Our results specify the long-held notion that “the evolutionary milieu in which taxa find themselves changed substantially” from the Palaeozoic to the modern world⁴⁹: We found a prominent decrease in environmental influence on the ecological success of marine calcifiers, although some 80 million years after the end of the Palaeozoic. This regime shift was caused by a number of abiotic and biotic revolutions in the Earth-Life system. Of all the factors contributing to this pattern, the onset of the modern carbon cycle via deep-sea CaCO₃ sedimentation was likely the most consequential for marine calcifying organisms. The high-

level taxonomic composition of marine life changed towards a “modern” biota after the end-Permian catastrophe¹, but the Palaeozoic evolutionary regime may have persisted well into the Mesozoic.

References

- 1 Alroy, J. The shifting balance of diversity among major marine animal groups. *Science* **329**, 1191-1194 (2010).
- 2 Bambach, R. K., Knoll, A. H. & Sepkoski, J. J. Anatomical and ecological constraints on Phanerozoic animal diversity in the marine realm. *Proceedings of the National Academy of Sciences* **99**, 6854-6859 (2002).
- 3 Finnegan, S., McClain, C. M., Kosnik, M. A. & Payne, J. L. Escargots through time: an energetic comparison of marine gastropod assemblages before and after the Mesozoic Marine Revolution. *Paleobiology* **37**, 252-269 (2011).
- 4 Heim, N. A., Knope, M. L., Schaal, E. K., Wang, S. C. & Payne, J. L. Cope’s rule in the evolution of marine animals. *Science* **347**, 867-870 (2015).
- 5 Payne, J. L., Heim, N. A., Knope, M. L. & McClain, C. R. Metabolic dominance of bivalves predates brachiopod diversity decline by more than 150 million years. *Proc. R. Soc. B* **281**, 20133122 (2014).
- 6 Ausich, W. I. & Bottjer, D. J. Tiering in Suspension-Feeding Communities on Soft Substrata throughout the Phanerozoic. *Science* **216**, 9 (1982).
- 7 Vermeij, G. J. The Mesozoic marine revolution: evidence from snails, predators and grazers. *Paleobiology* **3**, 245-258 (1977).
- 8 Vermeij, G. J. *Evolution and escalation: an ecological history of life*. (Princeton University Press, 1987).

184 9 Aberhan, M., Kiessling, W. & Fürsich, F. T. Testing the role of biological interactions in
185 the evolution of mid-Mesozoic marine benthic ecosystems. *Paleobiology* **32**, 259-277
186 (2006).

187 10 Sandberg, P. A. An oscillating trend in Phanerozoic non-skeletal carbonate mineralogy.
188 *Nature* **305**, 19-22 (1983).

189 11 Veizer, J., Godderis, Y. & François, L. M. Evidence for decoupling of atmospheric CO₂
190 and global climate during the Phanerozoic eon. *Nature* **408**, 698-701 (2000).

191 12 Ridgwell, A. A Mid Mesozoic Revolution in the regulation of ocean chemistry. *Marine*
192 *Geology* **217**, 339-357 (2005).

193 13 Bachan, A. *et al.* A model for the decrease in amplitude of carbon isotope excursions
194 across the Phanerozoic. *American Journal of Science* **317**, 641-676 (2017).

195 14 Alroy, J. Accurate and precise estimates of origination and extinction rates.
196 *Paleobiology* **40**, 374-397 (2014).

197 15 Balthasar, U. & Cusack, M. Aragonite-calcite seas—Quantifying the gray area. *Geology*
198 **43**, 99-102 (2015).

199 16 Hardie, L. A. Secular variation in seawater chemistry: An explanation for the coupled
200 secular variation in the mineralogies of marine limestones and potash evaporites over
201 the past 600 my. *Geology* **24**, 279-283 (1996).

202 17 Higuchi, T., Shirai, K., Mezaki, T. & Yuyama, I. Temperature dependence of aragonite
203 and calcite skeleton formation by a scleractinian coral in low mMg/Ca seawater.
204 *Geology* **45**, 1087-1090 (2017).

205 18 Ramajo, L., Rodríguez-Navarro, A. B., Duarte, C. M., Lardies, M. A. & Lagos, N. A. Shifts
206 in shell mineralogy and metabolism of *Concholepas concholepas* juveniles along the
207 Chilean coast. *Marine and Freshwater Research* **66**, 1147-1157 (2015).

208 19 Ries, J. Review: geological and experimental evidence for secular variation in seawater
209 Mg/Ca (calcite-aragonite seas) and its effects on marine biological calcification.
210 *Biogeosciences* **7**, 2795 (2010).

211 20 Harper, E. M., Palmer, T. J. & Alpey, J. Evolutionary response by bivalves to changing
212 Phanerozoic sea-water chemistry. *Geological Magazine* **134**, 403-407 (1997).

213 21 Porter, S. Calcite and aragonite seas and the *de novo* acquisition of carbonate
214 skeletons. *Geobiology* **8**, 256-277 (2010).

215 22 Demicco, R. V., Lowenstein, T. K., Hardie, L. A. & Spencer, R. J. Model of seawater
216 composition for the Phanerozoic. *Geology* **33**, 877-880 (2005).

217 23 Veizer, J. & Prokoph, A. Temperatures and oxygen isotopic composition of
218 Phanerozoic oceans. *Earth-Science Reviews* **146**, 92-104 (2015).

219 24 Hannisdal, B., Henderiks, J. & Liow, L. H. Long-term evolutionary and ecological
220 responses of calcifying phytoplankton to changes in atmospheric CO₂. *Global Change*
221 *Biology* **18**, 3504-3516 (2012).

222 25 Kiessling, W., Aberhan, M. & Villier, L. Phanerozoic trends in skeletal mineralogy driven
223 by mass extinctions. *Nature Geoscience* **1**, 527-530 (2008).

224 26 Foote, M., Crampton, J. S., Beu, A. G. & Nelson, C. S. Aragonite bias, and lack of bias,
225 in the fossil record: lithological, environmental, and ecological controls. *Paleobiology*
226 **41**, 245-265 (2015).

227 27 Sugihara, G. *et al.* Detecting causality in complex ecosystems. *science*, 1227079 (2012).

228 28 Knoll, A. H., Bambach, R. K., Payne, J. L., Pruss, S. & Fischer, W. W. Paleophysiology
229 and end-Permian mass extinction. *Earth and Planetary Science Letters* **256**, 295-313
230 (2007).

231 29 Grotzinger, J. P. & Knoll, A. H. Anomalous carbonate precipitates: is the Precambrian
232 the key to the Permian? *Palaios*, 578-596 (1995).

233 30 Langdon, C. *et al.* Effect of calcium carbonate saturation state on the calcification rate
234 of an experimental coral reef. *Global Biogeochemical Cycles* **14**, 639-654 (2000).

235 31 De Choudens-Sanchez, V. & Gonzalez, L. A. Calcite and aragonite precipitation under
236 controlled instantaneous supersaturation: elucidating the role of CaCO₃ saturation
237 state and Mg/Ca ratio on calcium carbonate polymorphism. *Journal of Sedimentary*
238 *Research* **79**, 363-376 (2009).

239 32 Webb, G. E. Was Phanerozoic reef history controlled by the distribution of non-
240 enzymatically secreted reef carbonates (microbial carbonate and biologically induced
241 cement)? *Sedimentology* **43**, 947-971 (1996).

242 33 Bown, P. R., Lees, J. A. & Young, J. R. in *Coccolithophores* 481-508 (Springer, 2004).

243 34 Ridgwell, A. & Zeebe, R. E. The role of the global carbonate cycle in the regulation and
244 evolution of the Earth system. *Earth and Planetary Science Letters* **234**, 299-315
245 (2005).

246 35 Clapham, M. E. & Renne, P. R. Flood Basalts and Mass Extinctions. *Annual Review of*
247 *Earth and Planetary Sciences* **47** (2019).

248 36 Wignall, P. B. *The Worst of Times: How Life on Earth Survived Eighty Million Years of*
249 *Extinctions*. (Princeton University Press, 2015).

250 37 Zeebe, R. E. & Westbroek, P. A simple model for the CaCO₃ saturation state of the
251 ocean: The “Strangelove,” the “Neritan,” and the “Cretan” Ocean. *Geochemistry,*
252 *Geophysics, Geosystems* **4** (2003).

253 38 Hudson, W., Hart, M. B. & Smart, C. W. Palaeobiogeography of early planktonic
254 foraminifera. *Bulletin de la Société géologique de France* **180**, 27-38 (2009).

255 39 Hart, M. B., Hudson, W., Smart, C. W. & Tyska, J. A reassessment of ‘Globigerina
256 bathoniana’Pazdrowa, 1969 and the palaeoceanographic significance of Jurassic
257 planktic foraminifera from southern Poland. *Journal of Micropalaeontology* **31**, 97-109
258 (2012).

259 40 Suchéras-Marx, B. *et al.* Impact of the Middle Jurassic diversification of Watznaueria
260 (coccolith-bearing algae) on the carbon cycle and $\delta^{13}\text{C}$ of bulk marine carbonates.
261 *Global and Planetary Change* **86**, 92-100 (2012).

262 41 Roth, P. H. Mesozoic palaeoceanography of the North Atlantic and Tethys oceans.
263 *Geological Society, London, Special Publications* **21**, 299-320 (1986).

264 42 Alroy, J. Dynamics of origination and extinction in the marine fossil record.
265 *Proceedings of the National Academy of Sciences* **105**, 11536-11542 (2008).

266 43 Clapham, M. E. Organism activity levels predict marine invertebrate survival during
267 ancient global change extinctions. *Global change biology* **23**, 1477-1485 (2017).

268 44 Falkowski, P. G. *et al.* The evolution of modern eukaryotic phytoplankton. *Science* **305**,
269 354-360 (2004).

270 45 Meyer, K., Ridgwell, A. & Payne, J. The influence of the biological pump on ocean
271 chemistry: implications for long-term trends in marine redox chemistry, the global
272 carbon cycle, and marine animal ecosystems. *Geobiology* **14**, 207-219 (2016).

- 273 46 Lu, W. *et al.* Late inception of a resiliently oxygenated upper ocean. *Science* **361**, 174-
274 177, (2018).
- 275 47 Vermeij, G. J. Escalation and its role in Jurassic biotic history. *Palaeogeography*,
276 *Palaeoclimatology, Palaeoecology* **263**, 3-8 (2008).
- 277 48 Vermeij, G. J. On escalation. *Annual Review of Earth and Planetary Sciences* **41**, 1-19
278 (2013).
- 279 49 Foote, M. Origination and extinction components of taxonomic diversity: Paleozoic
280 and post-Paleozoic dynamics. *Paleobiology* **26**, 578-605 (2000).

281

282 **Corresponding author**

283 Correspondence and requests for materials should be addressed to Kilian Eichenseer
284 (kilian.eichenseer@plymouth.ac.uk).

285

286 **Acknowledgements**

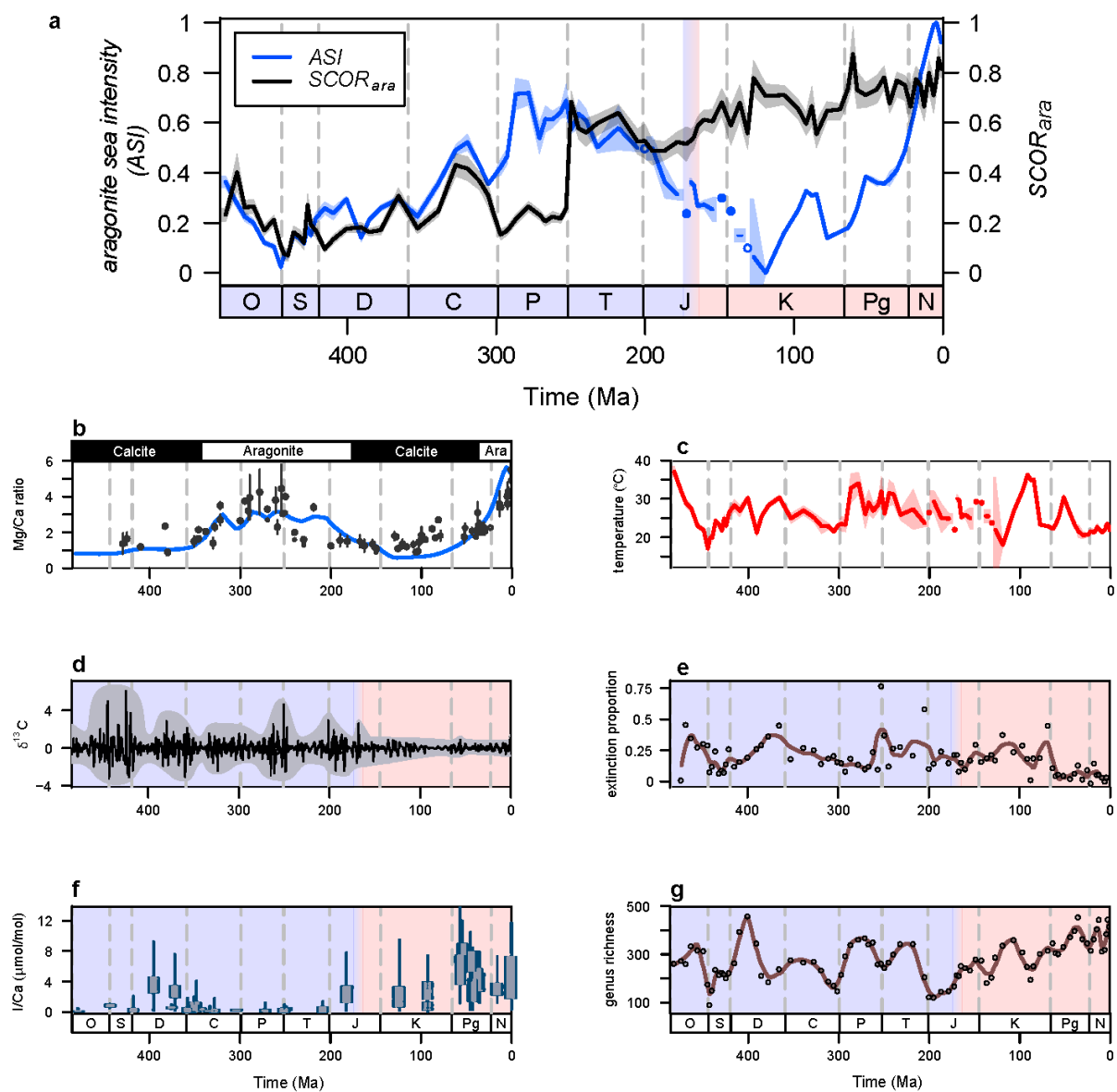
287 This project was supported by the University of Plymouth (K.E., U.B., C.W.S. and J.S.) , by the
288 Trond Mohn Foundation (funding to K.A.H.) and by the Deutsche Forschungsgemeinschaft (KI
289 806/16-1, funding to W.K.). We thank all contributors to the Paleobiology Database, and
290 David Diego for discussions on pullback attractor formalism and CCM interpretations. We are
291 grateful to James Crampton, Ashleigh Hood for their comments on an earlier version of this
292 manuscript. This is Paleobiology Database publication no. 344.

293 **Author contributions**

294 K.E., U.B., W.K. and C.W.S. designed the study. J.S. developed and implemented the Bayesian
295 changepoint regression analysis. K.A.H. performed the convergent cross mapping analysis.
296 K.E. carried out all other data analysis and wrote the initial manuscript draft, and all authors
297 contributed substantially to its improvement.

298 **Competing interests**

299 The authors declare no competing interests.

Figure 1**Figure 1: Environmental and biotic changes across the Ordovician – Neogene**

(a) *ASI* (aragonite sea intensity, blue) and $SCOR_{ara}$ (relative Summed Common species Occurrence Rate of aragonitic genera, black), in 85 Ordovician – Pleistocene stages. Shaded areas represent 2 standard errors around the mean with the *ASI* error envelope being based on the temperature component (*Methods*). Stages

with only one measurement are drawn as solid dots, stages without observations (circles) have been averaged from the neighboring stages.

Legend: O = Ordovician, S = Silurian, D = Devonian, C = Carboniferous, P = Permian, T = Triassic, J = Jurassic, K = Cretaceous, Pg = Palaeogene, N = Neogene and Quaternary, Ma = Million years ago. The blue – red transitions and the vertical bar mark the time when the relationship between *ASI* and *SCOR_{ara}* decreased most strongly (See Fig. 2b, c).

(b) Modelled Mg/Ca ratio from ref. 22 (blue line) and a compilation of Mg/Ca proxy data (black dots, see Supplementary Materials S1). The bar at the top delineates calcite and aragonite sea intervals as predicted by ref. 16.

(c) Mean stage-level tropical shallow water temperatures calculated from oxygen isotope measurements compiled in ref. 23. Stages with only one measurement are drawn as solid dots, stages without observations have been averaged from the neighbouring stages and are shown as circles. Shaded areas represent 2 standard errors around the mean.

(d) Periodic changes in the envelope of third-order $\delta^{13}\text{C}$ variations, reprinted from ref. 13 with permission of the American Journal of Science. The grey area highlights the variability.

(e) Genus-level, sampling-standardised extinction proportions (circles, see *Methods*) with long-term trend line (brown; LOESS regression with a smoothing span of 0.1).

(f) Box plots showing the variability of iodine-to-calcium (I/Ca) ratios from shallow water carbonates within sampling localities, reprinted from ref. 46 with permission from

329 AAAS. I/Ca ratios are considered a proxy for oxygenation, with higher I/Ca ratios
330 indicating better oxygenation.

331 (g) Sampling-standardised marine genus-level diversity (circles, see *Methods*) with long-
332 term trend line (brown; LOESS regression with a smoothing span of 0.1).

333

Figure 2

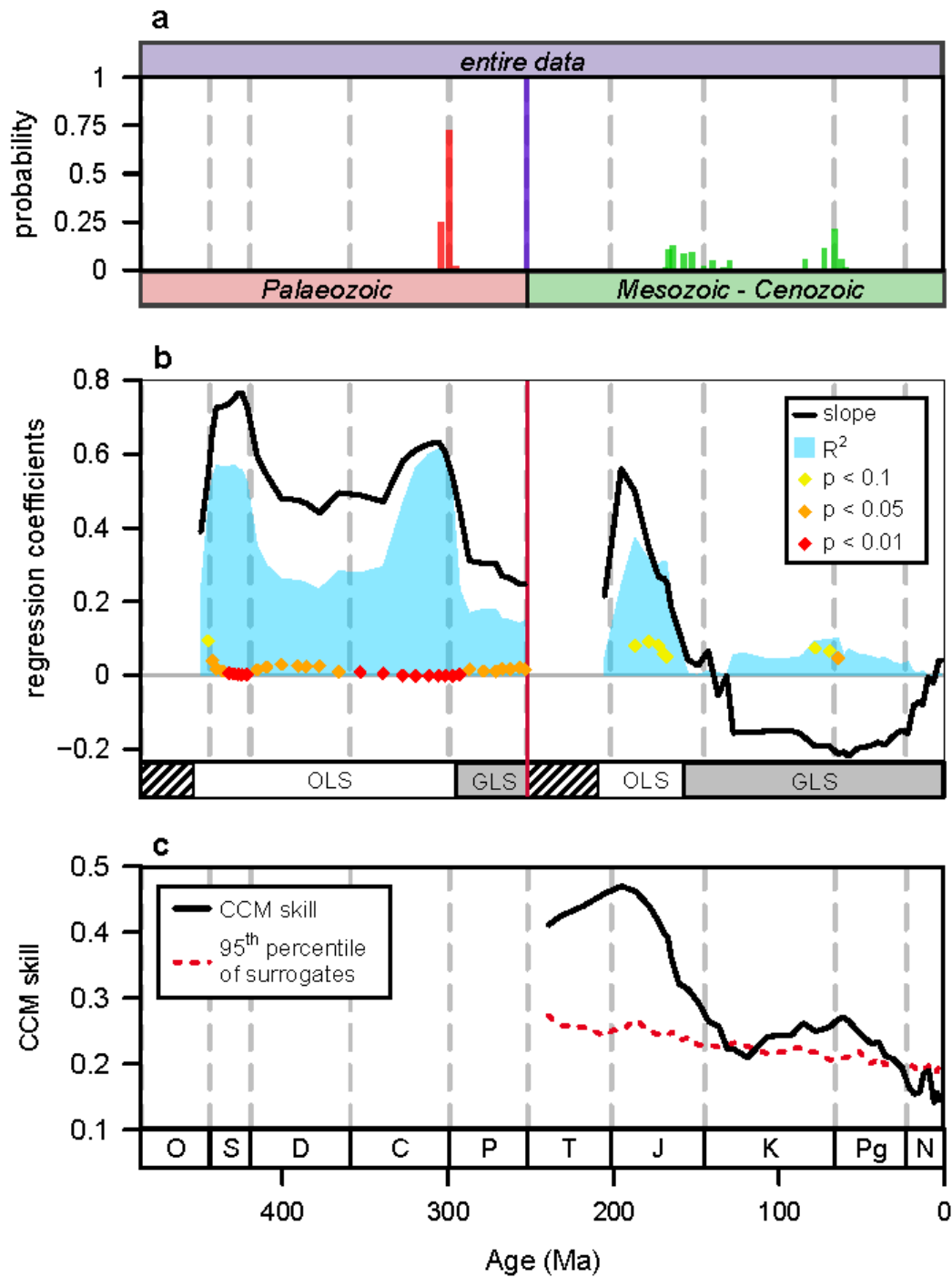


Figure 2: Changing relationship of $SCOR_{ara}$ and ASI .

(a) Bayesian posterior probabilities for changes in the linear regression of $SCOR_{ara}$ against ASI for the entire time series (purple bar), the Palaeozoic (red) and the Triassic – Pleistocene

(green). The strength of correlation between $SCOR_{ara}$ and ASI changed around the Carboniferous – Permian boundary and at the Permian – Triassic boundary, whereas no distinct point of change is found in the Mesozoic – Cenozoic time series.

(b) Linear models of $SCOR_{ara}$ against ASI in windows of increasing length for the Palaeozoic and for the Mesozoic – Cenozoic. Expanding windows start with the first six stages and all data are plotted at the last stage of the respective window. Black line = slope; blue area = R^2 ; diamonds = p-values; only p-values < 0.1 are shown. The boxes at the bottom of the graph indicate the gap for the first five stages (hatched pattern), and whether linear models were generated using ordinary least squares (OLS), or generalised least squares (GLS, *see Methods*). These results demonstrate a strong positive correlation between $SCOR_{ara}$ and ASI for the Palaeozoic time series, and a strong, although less robust positive correlation in the early Mesozoic that weakens with the inclusion of data from the Middle Jurassic onwards-

(c) Predicting ASI from $SCOR_{ara}$ with convergent cross mapping (CCM) for expanding time series. All included time series start with the first Ordovician stage and all data are plotted at the last stage of their respective window. The CCM prediction skills (solid black line) can be interpreted as the strength of dynamical influence of ASI on $SCOR_{ara}$. The dashed red line shows the 95th percentile of 500 random surrogate time series, which we take as a significance criterion. Time windows shorter than the Ordovician – Middle Triassic did not pass the CCM convergence test and were not included (*see Methods*). The CCM skill shows a sustained drop when Jurassic – Early Cretaceous stages are added, which implies a continuously weakening dynamical influence of ASI on $SCOR_{ara}$.

360 Tables

Table 1: Linear models with GLS

(d) Generalised least squares linear models of $SCOR_{ara}$ against ASI in the entire data set and in temporal subsets. N denotes the number of observations, ϵ denotes the error term of the regression, with AR indicating autoregressive errors and *ind.* indicating independent errors. ϕ denotes the autocorrelation of the error at lag = 1. In models with autocorrelated error terms, R^2 is calculated from the log-likelihoods of the model and the corresponding null model (*Methods*). Models with independent errors are equivalent to an ordinary least squares linear model.

	N	ϵ	ϕ	Intercept	Slope	R^2	p
entire data set	85	AR	0.93	0.45	0.05	0.00	0.70
Palaeozoic	38	AR	0.57	0.13	0.25	0.15	0.017
Ordovician - Carboniferous	29	<i>ind.</i>	-	0.07	0.60	0.59	< 0.001
Permian	9	<i>ind.</i>	-	0.05	0.28	0.68	0.006
Mesozoic - Cenozoic	47	AR	0.68	0.65	0.04	0.00	0.68

361

362

Methods

Fossil and palaeoenvironmental data were grouped into 85 Ordovician to Pleistocene geological stages. To achieve more uniform stage durations, we combined stages shorter than 1 million years (myr) with neighbouring stages (Table S4). Consequently, the two Early Triassic stages were combined, as were the four Pleistocene stages. All analyses were carried out in R, version 3.4.1⁵⁰

Fossil data. We used the Paleobiology Database (PBDB, <https://paleobiodb.org/>) to assess the global fossil record of marine calcifiers. The PBDB records occurrences of fossil organisms and the geological setting in which they were preserved. For our analysis, we relied on internal PBDB information on stratigraphy, taxonomy, mineralogy, life habits, preservation, lithification, and palaeocoordinates (Table S3). All Phanerozoic occurrence data were downloaded on 24 January 2017 with standard settings. Cambrian occurrences were later omitted as *ASI* could only be calculated in the Ordovician – Pleistocene due to the insufficient Cambrian palaeotemperature record. We also excluded occurrences from non-marine settings and occurrences that could not be assigned with confidence to a geological stage. We only included occurrences that were identified to genus level and that could be reliably assigned to an invertebrate animal phylum, Foraminifera, Chlorophyta, Rhodophyta, or calcifying “Problematica”. Occurrences of plankton (coccolithophores, planktonic foraminifera, planktonic gastropods or planktonic tentaculites) were omitted. We followed the classification of skeletal mineralogy in the PBDB and considered calcifiers as “aragonitic” if their dominant mineralogy was aragonite and no secondary mineral was listed. The skeletal mineralogies recorded in the PBDB are based on the protocol described in ref. 25, from which we deviated in few exceptions – labechiid and Palaeozoic chaetetid sponges were classified as possessing a high Mg calcite skeleton (Balthasar *et al.*, unpublished).

As aragonite is thermodynamically unstable at Earth surface conditions and eventually dissolves or recrystallizes to calcite, aragonite has a lower preservation potential than calcite^{26,51}. Most occurrences of aragonite preservation are therefore concentrated in the youngest stages. We

minimized this time-dependant bias by excluding all occurrences from collections with aragonite preservation and unlithified sediments, but kept the 19 % of data which had no information on their preservation recorded to avoid excessive loss of fossil data (see Supplementary Text S3). Barring some potential undeclared occurrences of aragonite preservation, the record of aragonitic taxa used herein thus consists of specimens that have been recrystallized to the stable calcite polymorph or that have been preserved in another way, e.g. by silicification.

Aragonite sea intensity (ASI). We developed a proxy for the degree to which aragonite precipitation is favoured relative to calcite precipitation in the non-biogenic environment based on the joint influence of temperature (T) and the Mg/Ca ratio on CaCO_3 formation in experiments⁵². We conducted a multiple linear regression of the mole percent of aragonite present in every experiment against the temperature and Mg/Ca ratio under which the experiments were conducted (see figure 1 in ref. 15). We only used experiments that produced > 1 % calcite and > 1 % aragonite. This yields the equation

$$(1) \text{ ASI} = -119.61 + 46.57 \times \frac{\text{Mg}}{\text{Ca}} + 4.30 \times T$$

To infer past *ASI* for the Ordovician – Pleistocene, palaeotemperatures were calculated from a Phanerozoic $\delta^{18}\text{O}$ compilation²³, including only measurements from fossil brachiopods, bivalves and planktonic foraminifera from 35° south to 35° north, because measurements from higher latitudes are unavailable for most of the Phanerozoic. For the $\delta^{18}\text{O}$ (‰ PDB) to $T(^{\circ}\text{C})$ transfer function, we calculated palaeotemperatures assuming a Phanerozoic trend of increasing $\delta^{18}\text{O}$ as in equation (2) from ref. 23. The Mg/Ca ratio ratios were taken from a Phanerozoic model of seawater composition and digitised from fig. 2.A of ref. 22 in steps of 2 million years using the R package *digitize*. For the Mg/Ca data, the mean from all observations falling into a geological stage was taken. *ASI* was calculated with average Mg/Ca data and with every individual temperature observation using equation (1). Mean and standard error of all *ASI* were calculated for each stage, and the resulting *ASI* was normalised to values between 0 and 1. No temperature data was available for the Hettangian and for the Hauterivian stage. We

413 calculated *ASI* for these stages with the mean temperature of the two neighbouring stages,
414 respectively.

415 **SCOR_{ara}**. Evolutionary success is widely assessed by diversity. Although species diversity and
416 abundance of higher taxonomic ranks or ecological groups are tightly coupled⁵³, we prefer a direct
417 measure of occupancy to assess the ecological success of individual genera. We apply the Summed
418 Common species Occurrence Rate (SCOR), which is driven by the most widespread and common
419 taxa²⁴. SCOR reflects the actual abundance of a group of taxa with good accuracy⁵⁴. The cumulative
420 SCOR of a set of m genera is calculated as

421
$$(2) \text{ SCOR} = \sum_{i=1}^m -\ln(1 - \frac{y_i}{k})$$

422 where genus i is present in y_i subsets out of a total of k occupied localities. We defined a locality as a
423 cell in a global penta-hexagonal grid with 6240 hexagonal and 12 pentagonal grid cells, with an area
424 of ca. 40,800 km². The grid was generated using the hexagrid() function in the icoso package⁵⁵. The
425 contribution of a genus to SCOR thus depends solely on the number of cells it was sampled in.
426 Repeated sampling within a cell does not increase SCOR. *SCOR_{ara}* reflects the ecological occupancy of
427 aragonitic taxa, relative to all calcifiers occurring at k_{all} localities. *SCOR_{ara}* is generated by dividing the
428 SCOR of aragonitic taxa with $k = k_{all}$ by the SCOR of all calcifying genera, again with $k = k_{all}$. To get the
429 relative success of major taxonomic groups, we divided the group SCOR by the SCOR of all calcifiers.
430 For every stage, we calculated SCOR using all genera recorded in the PBDB fossil data recorded in that
431 respective stage.

432 We calculated the variance of any SCOR metric with the delta method^{24,56}

433
$$(3) \text{ Var(SCOR)} = \sum_{i=1}^m \frac{\frac{y_i}{k}}{(1 - \frac{y_i}{k})^{*k}}$$

434 and can approximate the variance of *SCOR_{ara}* using the means and variance of aragonitic SCOR and the
435 SCOR of all calcifiers, assuming they are independent:

436 (4) $\text{Var}(\text{SCOR}_{ara}) = \left(\frac{\text{aragonitic SCOR}}{\text{all calcifier SCOR}}\right)^2 \times \left(\frac{\text{Var}(\text{aragonitic SCOR})}{\text{aragonitic SCOR}} + \frac{\text{Var}(\text{all calcifier SCOR})}{\text{all calcifier SCOR}}\right).$

437 **Bayesian change point regression analysis.** The relationship of ASI and SCOR_{ara} changed through time.

438 We developed statistical methodology to identify change points. In particular, we performed

439 inference in the Bayesian framework about the unknown parameters of the model $y_i \sim N(\mu_i, \sigma_i^2)$,

440 $i = 1, \dots, n$, independently, in which n is the overall sample size and

441 (5)
$$\mu_i = \begin{cases} \alpha_1 + \beta_1 x_i & i = 1, \dots, n_1 \\ \sum_{j=1}^2 \alpha_j + \sum_{j=1}^2 \beta_j x_i & i = n_1 + 1, \dots, n \end{cases}$$

442 This model allows a distinct linear relationship between y_i and the covariate x_i in a first and second

443 part of the time series. The parameter α_2 and β_2 represent the additional intercept and slope in the

444 second part, added to α_1 and β_1 of the first part. $\log \sigma_i$ is defined in a similar way, allowing for a

445 different relationship between the standard deviation σ_i and the covariate x_i in each time series part.

446 In the Bayesian framework, it is necessary to specify prior distributions for all unknown parameters.

447 We adopted normal priors with very high variances for all intercept and slope parameters. For the

448 change point n_1 , we adopted a discrete uniform prior across integer values from 5 to $n - 5$, implying

449 that the change point divides the time series into two sections with at least five data points each. This

450 prior distribution expresses considerable uncertainty about the position of the change point before

451 seeing the data. As it is impossible to handle the posterior distribution of all these parameters

452 analytically, we followed the standard approach of sampling from this distribution using a Markov

453 chain Monte Carlo (MCMC) algorithm⁵⁷. To do this we used the jags program⁵⁸, accessed in R through

454 the R2jags package⁵⁹. Our posterior inference is based on 100,000 iterations of the MCMC algorithm,

455 half of which were discarded as burn-in.

456 After inferring a first change point at the Permian-Triassic boundary, we split the data set into a

457 Palaeozoic part and a Mesozoic – Cenozoic part. In each of the two parts, we estimated additional

458 change points with the method described above.

459 **Generalised least squares.** Linear regression with ordinary least squares (OLS) of the form

460
$$(6) \quad y = \alpha + \beta x + \varepsilon$$

461 assumes that the errors ε are independent between observations. For our data, the residuals of an
462 OLS linear model of $SCOR_{ara}$ against ASI are autocorrelated, which suggests that this assumption of
463 independent errors does not hold. Generalised least square regression (GLS) can incorporate
464 autoregressive errors and thus allows us to test for linear relationships between autocorrelated time
465 series⁶⁰. Autocorrelated errors ε of order p can be modelled as

466
$$(7) \quad \varepsilon_i = \sum_{j=1}^p \phi_j \varepsilon_{i-j} + \delta_i$$

467 with $\delta_i \sim N(0, \sigma^2)$ independently, in which σ is the standard deviation. We created linear models with
468 independent and with autocorrelated error terms of the first order using the `gls()` function of the nlme
469 R package⁶¹, performing maximum likelihood estimation by specifying `gls(..., method = "ML")`. For
470 model selection we compared pairs of models with and without autoregressive errors using a
471 likelihood ratio test⁶², implemented using the `anova.gls()` function. We selected the more complicated
472 model only if the associated p-value was < 0.05 and the likelihood ratio was > 1 . In a few instances,
473 models with autocorrelated errors estimated $\phi < 0$, which we attributed to model overfitting. In these
474 cases, we chose the model without autocorrelation.

475 As a goodness-of-fit measure for GLS models, we calculated the likelihood ratio test R^2 as

476
$$(8) \quad R^2 = 1 - \exp\left(-\frac{2}{m}(\log L_M - \log L_0)\right)^{63,64},$$

477 with m being the number of observations, $\log L_M$ being the log-likelihood of the model, and $\log L_0$ being
478 the log-likelihood of the null model of the form $y = 1 + \varepsilon$, with ε being the error as in equation (7).

479 We take 0.05 as the alpha level for the statistical significance of linear regressions.

480 **Regression in expanding windows.** We assessed the changing strength of a relationship between ASI
481 and $SCOR_{ara}$ through time by calculating linear models in windows of expanding length. Due to the

severe increase of $SCOR_{ara}$ across the Permian-Triassic boundary, calculating the linear relationship across the entire data set may be misleading. Instead, linear models were formulated separately in the Palaeozoic and Mesozoic-Cenozoic. In both cases, the shortest window considered comprised the first six data points, while the longest window had 38 points in the Palaeozoic and 47 points in the Mesozoic – Cenozoic. In every window, an OLS and a GLS model was fitted, with autoregressive errors of the first order incorporated into the GLS model. GLS models were used from the first window onwards in which ϕ was positive and a likelihood ratio test comparing the OLS and the GLS model produced a p -value < 0.05 .

Convergent cross mapping. The success of marine calcifiers may be influenced by environmental parameters other than climate and ocean chemistry, as well as biotic interactions and chance. It is therefore possible that a causal connection between ASI and $SCOR_{ara}$ exists even when no linear relationship is detected. We test for this possibility using CCM, a model-free time series analysis method based in dynamical systems theory that can detect causal coupling in nonlinear and even chaotic systems²⁷. It asserts that if two processes are causally linked, then information about the driver variable can be recovered from the response variable²⁷. CCM indirectly measures the dynamical influence of the driver variable on the response variable by quantifying the extent to which a state space reconstruction (time delay embedding) of the response variable can be used to predict the driver time series. A description of the algorithm can be found in the Supplementary Materials (S2).

To test for a temporally variable influence of ASI on $SCOR_{ara}$, we performed CCM analysis on expanding time windows on the stage level data, under the assumption that these coarse-grained data contain sufficient dynamical information about Phanerozoic Earth system dynamics (see Supplementary Materials S2). We used the rEDM R package⁶⁵ to perform CCM analyses for the main paper. Because of the limited number of time series points, we used embedding dimension 2 and embedding lag 1, with zero temporal exclusion radius in the predictions due to the coarse temporal resolution of the data. For a given time window, the CCM analysis is convergent if prediction skill

increases with increasing library size (Supplementary Materials S2). If convergence is achieved, for each time window of length L , we report the median CCM skill for 500 bootstrapped samples at a library size L . In addition, to assess the significance of the results, we used surrogate testing with randomly shuffled surrogates⁶⁶. The analysis for a given time window was considered significant if the median prediction skill at the largest library size exceeded the 95th percentile of the median prediction skills obtained for an ensemble of 500 surrogate CCM analyses (dashed, red line in Fig. 2c), where each surrogate realization, the driver time series is replaced by a randomly shuffled version of itself.

Diversity dynamics. We calculated second-for-third extinction proportions⁶⁷ using classical rarefaction^{14,68} with a sampling quota of 500 occurrences per stage and took the mean extinction proportions over 100 subsampling trials. A sampling-standardised diversity curve was generated with shareholder-quorum subsampling¹ by taking the mean of 100 subsampling iterations, each with a quorum of 0.7. Following the recommendations in ref. 1, we relied on the reference-based singleton count, excluded the dominant genus from frequency calculations, and excluded the largest collection from the single-publication occurrence count. To control for short-term sampling variation, we used the corrected sampled-in-bin richness metric⁶⁹, except for the first and the last stage, in which no sampling correction could be made. A locally estimated scatterplot smoothing (LOESS) regression⁷⁰ has been calculated from these results using a smoothing span of 0.1. Extinction and diversity computations were performed using the divDyn R package⁷¹.

Data availability

The data used to calculate $SCOR_{ara}$ are available from the Paleobiology Database at <https://paleobiodb.org/>. The data used to calculate aragonite sea intensity were taken from ref. 15, 22, and 23.

Code availability

The code used to generate the results can be accessed at https://figshare.com/articles/R_scripts_and_protocols/7199561.

Methods only References

50 R Core Team. R: A Language and Environment for Statistical Computing. <https://www.R-project.org/> (2017).

51 Cherns, L. & Wright, V. P. Quantifying the impacts of early diagenetic aragonite dissolution on the fossil record. *Palaios* **24**, 756-771 (2009).

52 Balthasar, U. *et al.* Relic aragonite from Ordovician–Silurian brachiopods: Implications for the evolution of calcification. *Geology* **39**, 967-970 (2011).

53 Madin, J. S. *et al.* Statistical independence of escalatory ecological trends in Phanerozoic marine invertebrates. *Science* **312**, 897-900 (2006).

54 Hannisdal, B., Haaga, K. A., Reitan, T., Diego, D. & Liow, L. H. Common species link global ecosystems to climate change: dynamical evidence in the planktonic fossil record. *Proc. R. Soc. B* **284**, 20170722 (2017).

55 Kocsis, Á. T. The R package icoso: Coarse resolution global triangular and pentahexagonal grids based on tessellated icosahedra. R package version 0.9.81. <https://CRAN.R-project.org/package=icoso> (2017).

56 Casella, G. & Berger, R. L. *Statistical inference*. Vol. 2 (Duxbury Pacific Grove, CA, 2002).

57 Brooks, S., Gelman, A., Jones, G. & Meng, X.-L. *Handbook of markov chain monte carlo*. (CRC press, 2011).

58 Plummer, M. JAGS Version 3.3. 0 user manual. *International Agency for Research on Cancer, Lyon, France* (2012).

554 59 Su, Y. & Yajima, M. R2jags: Using R to run 'JAGS'. R package version 0.5–7.
555 <https://CRAN.R-project.org/package=R2jags> (2015).

556 60 Faraway, J. J. *Linear models with R*. (CRC press, 2014).

557 61 Pinheiro, J. *et al.* nlme: Linear and Nonlinear Mixed Effects Models. R package version
558 3.1-131. <https://CRAN.R-project.org/package=nlme> (2017).

559 62 Davison, A. C. *Statistical models*. Vol. 11 (Cambridge University Press, 2003).

560 63 Kramer, M. R 2 statistics for mixed models. *Presented at the 17th Annual Kansas State*
561 *University Conference on Applied Statistics in Agriculture, Manhattan, Kansas, 24–26*
562 *April* (2005).

563 64 Magee, L. R 2 measures based on Wald and likelihood ratio joint significance tests. *The*
564 *American Statistician* **44**, 250-253 (1990).

565 65 Ye, H., Clark, A., Deyle, E., Keyes, O. & Sugihara, G. *rEDM: Applications of empirical*
566 *dynamic modeling from time series*. R Package Version 0.5 7. [https://CRAN.R-](https://CRAN.R-project.org/package=rEDM)
567 [project.org/package=rEDM](https://CRAN.R-project.org/package=rEDM) (2017).

568 66 Theiler, J., Eubank, S., Longtin, A., Galdrikian, B. & Farmer, J. D. Testing for nonlinearity
569 in time series: the method of surrogate data. *Physica D* **58**, 77–94 (1992).

570 67 Alroy, J. A more precise speciation and extinction rate estimator. *Paleobiology* **41**, 633-
571 639 (2015).

572 68 Sanders, H. L. Marine benthic diversity: a comparative study. *The American Naturalist*
573 **102**, 243-282 (1968).

574 69 Alroy, J. *et al.* Phanerozoic trends in the global diversity of marine invertebrates.
575 *Science* **321**, 97-100 (2008).

576 70 Cleveland, W. S., Grosse, E., Shyu, W. M., Chambers, J. M. & Hastie, T. Statistical
577 models in S. *Local regression models*, Chapter 8 (1992).

578 71 Kocsis, Á. T., Reddin, C. J., Alroy, J. & Kiessling, W. The r package divDyn for quantifying
579 diversity dynamics using fossil sampling data. *Methods in Ecology and Evolution* **10**,
580 735-743 (2019).